# Image Cover Sheet

| CLASSIFICATION | SYSTEM NUMBER |
| --- | --- |
| UNCLASSIFIED | 510080 |

**TITLE**

MULTIPLE SCATTERING IN LIDAR REMOTE SENSING: NUISANCE AND BENEFIT

**System Number:**

**Patron Number:**

**Requester:**

**Notes:**

**DSIS Use only:**

**Deliver to:**

PROCEEDINGS OF SPIE REPRINT

EUROPTO SERIES

*Reprinted from*

# *Atmospheric Propagation, Adaptive Systems, and Lidar Techniques for Remote Sensing II*

**23–24 September 1998**
**Barcelona, Spain**


**Volume 3494**

# Multiple scattering in lidar remote sensing: nuisance and benefit

Luc R. Bissonnette, Gilles Roy,

DREV-Defence Research Establishment Valcartier
2459, Pie XI Blvd. North, Val-Bélair, Québec, Canada, G3J 1X5
*Tel.*: +418-844-4437 • *Fax*: +418-844-4511 • *E-mail*: luc.bissonnette@drev.dnd.ca
and Shiv Pal
Centre for Research in Earth and Space Technology
4850 Keele Street, North York, Ontario, Canada M3J 3K1

## ABSTRACT

The paper discusses adverse and favorable effects of multiple scattering in lidar measurements. Adverse effects arise because the conventional lidar equation ignores multiply scattered radiation. Hence, the parameters retrieved under this approximation are in error by an amount that depends on the multiple scattering strength. This is illustrated by numerical simulations of space-based DIAL measurements of atmospheric ozone profiles in the presence of cirrus clouds and ground layer aerosols. On the other hand, multiple scattering contributes additional information on the aerosol extinction coefficient and particle size. The paper shows that this can be exploited to derive simultaneous solutions for the extinction coefficient and mean particle diameter independently of external data as required in conventional solution methods.
*Key words:* Lidar, multiple scattering, aerosols

## 1. INTRODUCTION

Remote sensing capabilities have long been sought to measure and characterize our environment. Among the available technologies, the lidar for Light Detection And Ranging has produced a diversity of useful data. Lidar began with searchlights to study stratospheric aerosols and molecular density.[1,2] The invention of the laser in 1960, particularly the Q-switched pulsed laser, rapidly opened the way to technological innovations and developments in atmospheric probing.

Most lidar works to date are based on the single scattering approximation whereby the only scattering that contributes to the measured return is the backscattering at 180°, all other scatterings being considered as losses. Following this model, the measured elastic backscattered signal $P$ from range $R$ is given by

$$P(R) = K\,F(R)\,P_0\,\frac{A}{R^2}\,\frac{ct}{2}\,\beta(R)\,\exp\left[-2\int_0^R \alpha(r)\,\mathrm{d}r\right], \tag{1}$$

where $K$ is the instrument constant, $F(R)$ is the transceiver overlap function, $P_0$ is the average laser pulse power, $A/R^2$ is the solid angle subtended by the receiver aperture $A$ for the radiation backscattered at range $R$, $ct/2$ is the range resolution with $c$ the speed of light and $t$ the laser pulse duration, and $\beta(R)$ and $\alpha(R)$ are the sums of the molecular and aerosol backscattering and extinction coefficients, respectively.

In reality, lidar measurements are affected in various ways by multiple scattering contributions that are not taken into account by Eq. 1. These effects have been recognized for quite some time, for example by Liou and Schotland,[3] Platt[4] and Pal and Carswell,[5] but have remained largely neglected. Although this approximation is justified in many applications, we will show here that multiple scattering can be either the source of important solution errors, or the carrier of valuable information.

The main difficulty in correcting for or taking advantage of multiple scattering in lidar applications has been the lack of suitable models and measurement methods. The situation, however, is gradually improving. Over the past few years, an informal international cooperation group, called MUSCLE for Multiple Scattering Lidar Experiments, has met on a semi-regular basis to join efforts toward developing reliable models and retrieval methods for multiply scattered lidar returns. A recent achievement of the group has been the publication of a dedicated issue of *Applied*

Part of the EUROPTO Conference on Laser Radar Techniques (Ranging and Atmospheric Lidar) II
Barcelona, Spain • September 1998
SPIE Vol. 3494 • 0277-786X/98/$10.00

*Physics B*[6] that contains contributions by various groups and a joint article[7] summarizing and discussing the results of a models intercomparison. Many of the ideas and concepts used in this paper have their origin in the articles of this special *Applied Physics B* issue and the series of MUSCLE conferences.

## 2. NUISANCE

Equation 1 shows that lidar returns, even in the simple single scattering approximation, depend on a multiplicity of atmospheric parameters. Measurements and data analysis techniques have been developed to get around this difficulty. For example, we can cite the doppler lidar technique that makes use of aerosol particles only as tracers for calculating the wind velocity from the optical frequency content of the return signals, the high spectral resolution[8] and Raman[9] lidars that separate the backscattering and extinction coefficients by splitting the molecular and aerosol backscatters and assuming known or independently measured the atmospheric molecular profile, and the differential absorption technique (DIAL) that relies only on the relative strength of two closely separated returns at two different wavelengths. These techniques have proved quite successful in inverting Eq. 1 for the retrieval of important atmospheric parameters. However, it is not yet well established how multiple scattering affects the precision of the solutions.

We consider here the errors induced by multiple scattering on DIAL solutions. To this end, we use the results recently published by Pal et Bissonnette.[10] Pal and Bissonnete conducted a simulation of space-based DIAL measurements of the stratospheric and tropospheric ozone at the on/off wavelengths of 305 and 315 nm; here 'on' refers to the wavelength most absorbed by ozone and 'off' to the one least absorbed. The air density, ozone concentration and aerosol profiles were specified over a 100-km deep atmosphere. They were kept constant except in the planetary boundary layer (bottom 3 km) where the aerosol profiles were matched to different ground aerosols and visibilities. In some of the computation runs, model cirrus clouds of diverse composition, optical densities and thicknesses were added at a height of 12 km. The lidar altitude was set at 300 km, the beam divergence at 0.1 mrad, and the receiver field of view at 0.5 mrad. The calculations were performed with the analytical model of Bissonnette[11] modified by the equivalence theorem of Katsev *et al.*[12] and extended to take into account the geometrical optics scatterings by the aerosol particles. Sample calculated returns are shown in Fig. 1, for a low ground visibility of 5 km in the left panel, and a high ground visibility of 25 km with a cold cirrus layer of unit optical thickness in the right panel.

The conventional ozone retrieval algorithm is based on Eq. 1 in which the backscattering coefficient is written as the sum of the molecular and aerosol components

$$\beta(R) = \beta_m(R) + \beta_a(R)\,, \tag{2}$$

and the extinction coefficient as the sum of the ozone, molecular and aerosol components

$$\alpha(R) = \alpha_{O_3}(R) + \alpha_m(R) + \alpha_a(R)\,. \tag{3}$$

The basis of the DIAL method consists in recording in rapid succession two lidar returns at the alternate wavelengths $\lambda_{on}$ and $\lambda_{off}$. $\lambda_{on}$ and $\lambda_{off}$ are chosen for large differences in $\alpha_{O_3}$ and minimal differences in $\alpha_m$ and $\alpha_a$. The ozone concentration $N_{O_3}$ is calculated from the ratio of the two returns $P_{on}$ and $P_{off}$ or more precisely by the following expression derived from Eq. 1:

$$N_{O_3} = \frac{1}{2(\Delta\sigma_{O_3})}\left\{\frac{\mathrm{d}}{\mathrm{d}R}\ln\left[\frac{P_{off}(R)}{P_{on}(R)}\right]\right\} - T_m - T_\beta - T_a\,, \tag{4}$$

where $\Delta\sigma_{O_3} = \sigma_{O_3,on} - \sigma_{O_3,off}$ is the differential ozone absorption cross-section, and $T_m$, $T_\beta$ and $T_a$ are correction terms resulting from

a) differential molecular extinction

$$T_m = \frac{1}{\Delta\sigma_{O_3}}[\alpha_{m,on} - \alpha_{m,off}]\,; \tag{5}$$

b) differential backscattering

$$T_\beta = \frac{1}{2\,\Delta\sigma_{O_3}}\frac{\mathrm{d}}{\mathrm{d}R}\ln\left[\frac{\beta_{off}(R)}{\beta_{on}(R)}\right]\,; \tag{6}$$

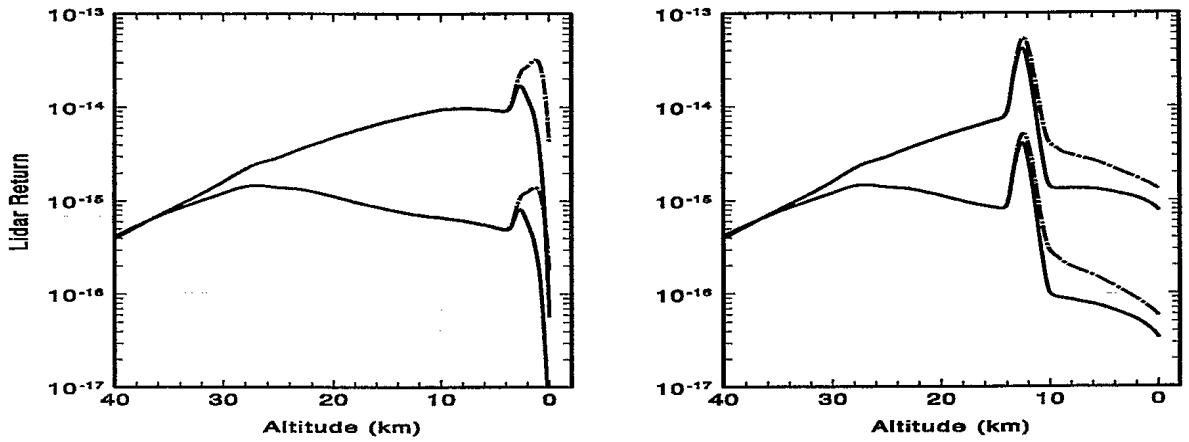


**Figure 1.** Simulated lidar returns from a space-based platform at 300 km at the ozone on and off wavelength of 305 and 315 nm. Continuous curves: single scattering; dot-dashed curves: multiple scattering. Left panel: 5-km visibility maritime aerosol ground layer; right panel: 25-km visibility ground layer with 2-km deep cold cirrus of Gaussian profile and unit optical thickness at an altitude of 12 km.

c) and differential aerosol extinction

$$T_a = \frac{1}{\Delta\sigma_{O_3}}[\alpha_{a,on} - \alpha_{a,off}]. \tag{7}$$

The correction term $T_m$ is calculable with good precision from measured atmospheric temperature and pressure profiles or from an appropriate model. The other two terms depend on aerosol concentration, size distribution and composition. These are variable quantities that are generally not known. In normal situations, $T_\beta$ and $T_a$ are negligible in the stratosphere and for the most part of the troposphere. However, in the lower troposphere and in the stratosphere following volcanic eruptions, $T_\beta$ and $T_a$ can be substantial and corrections algorithms need to be implemented, for example as discussed by Steinbrecht and Carswell.[13]

Equation 4 is based on the single scattering lidar equation 1. Therefore, in addition to the three correction terms given above, we need to consider a fourth error source due to multiple scattering. Since there is yet no analytic model of multiple scattering, the correction cannot be explicitly expressed as was done for $T_m$, $T_\beta$ and $T_a$. What we will do here is use Eq. 4 to calculate $N_{O_3}$ from the numerically simulated multiply scattered $P_{ms,on}$ and $P_{ms,off}$, and compare the retrieved profiles with the true $N_{O_3}$ profile used to generate $P_{ms,on}$ and $P_{ms,off}$. The differences will give an estimate of the magnitude of the multiple-scattering-induced errors that could be expected in actual measurements. In particular, we want to compare these errors with $T_\beta$ and $T_a$ as it has been suggested by Wandinger[14] that they might be of second order.

To establish a baseline, we have first performed the calculations with the simulated single scattering returns. For example, the retrieved $N_{O_3}$ profiles for the high and low visibility tropospheric maritime aerosol cases are plotted in the left and right panels of Fig. 2, respectively. The differential molecular extinction correction term $T_m$ was subtracted in both cases but not the aerosol-dependent $T_\beta$ and $T_a$ because the relevant aerosol properties are not known in most DIAL measurements. We see that the overestimation errors induced by the aerosol effects are negligible in the stratosphere but quite substantial in the troposphere, particularly in the planetary boundary layer where the aerosol loading is higher. Similar errors could also be expected in the stratosphere in the months and even years following strong volcanic eruptions.

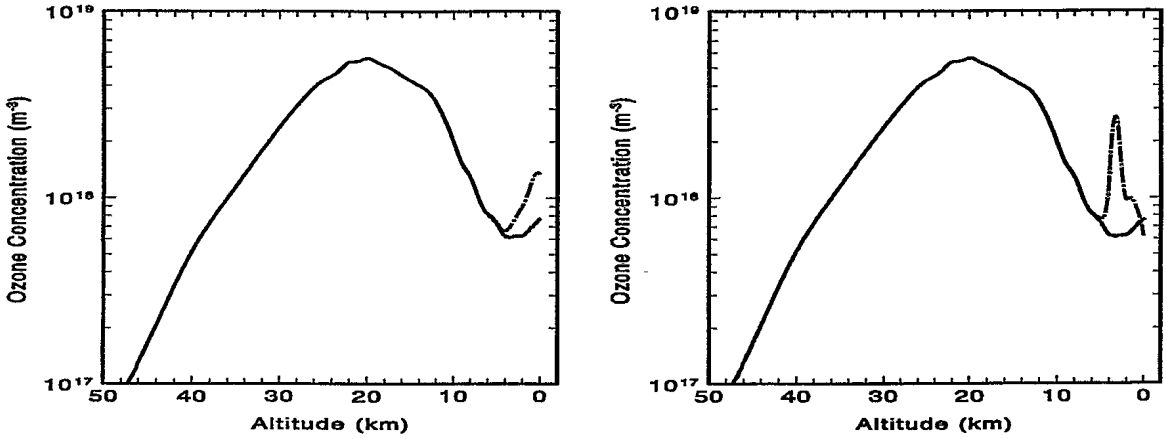


**Figure 2.** Ozone concentration profiles (dot-dashed curve) retrieved from simulated single scattering lidar returns with $T_m$ correction applied compared with true profile (continuous curve). Left panel: 25-km ground layer visibility; right panel: 5-km ground visibility.

To isolate the effect of multiple scattering, we will from here on subtract all three explicit single scattering correction terms, which is not only possible but straightforward to do in the case of simulations. Figure 3 shows the ratio of the retrieved $N_{O_3}$ profiles to the true profiles for the same cases as plotted in Fig. 2 but, this time, calculated from the multiply scattered returns $P_{ms,on}$ and $P_{ms,off}$. There is no measurable error in the stratosphere but, in the planetary boundary layer, we find a small error of less than 5% and a larger error of more than 60% for the high and low visibility conditions, respectively. Although somewhat smaller than the single scattering aerosol errors of Fig. 2, the multiple scattering effects of Fig. 3 are nevertheless important and could not be ignored in space-based DIAL measurements of tropospheric ozone.

Two more examples of ozone retrieval errors, caused in this case by multiply scattered radiation contributed by a cirrus cloud layer, are shown in Fig. 4. In both figures, the cold cirrus has an optical depth of unity and is centered at an altitude of 12 km; the geometrical thickness ($e^{-1}$ points of the assumed Gaussian profile) is 2 km for the left panel and 4 km for the right panel. The retrieved $N_{O_3}$ profiles go through a large overestimation-underestimation oscillation and then rapidly settle to whithin a few percent of the true value. The oscillation begins well into the cloud, at a point where the crystal density is about 60% of its maximum value, and ends with vanishing cloud density. With reference to the right panel of Fig. 1, we can see that the main error appears where multiple scattering begins to make a difference but disappears as soon as the pulse emerges at cloud base despite the fact that the relative strength of the multiple scattering contributions peaks there and remains high down to the earth surface.

Multiple scattering increases the amount of available radiation but the results of Fig. 1 and 4 show that this is not sufficient to cause DIAL errors. There must also be wavelength-dependent differences in the particle properties that govern the scattering of these additional photons back into the receiver. The significant retrieval errors cease where the multiple-scattering-enhanced pulse leaves the cloud and re-enters a region of minimal differences in aerosol properties. Actually, these simulations show that, outside of cloud regions, accurate ozone profiles could still be retrieved from space even through cirrus clouds.

The mutiple scattering DIAL errors have basically the same origin as the single scattering errors, namely the wavelength dependence of the driving aerosol properties, and they have more or less the same importance, at least in the problem treated here. Our simulation results indicate that where there is sufficient aerosol loading, whether

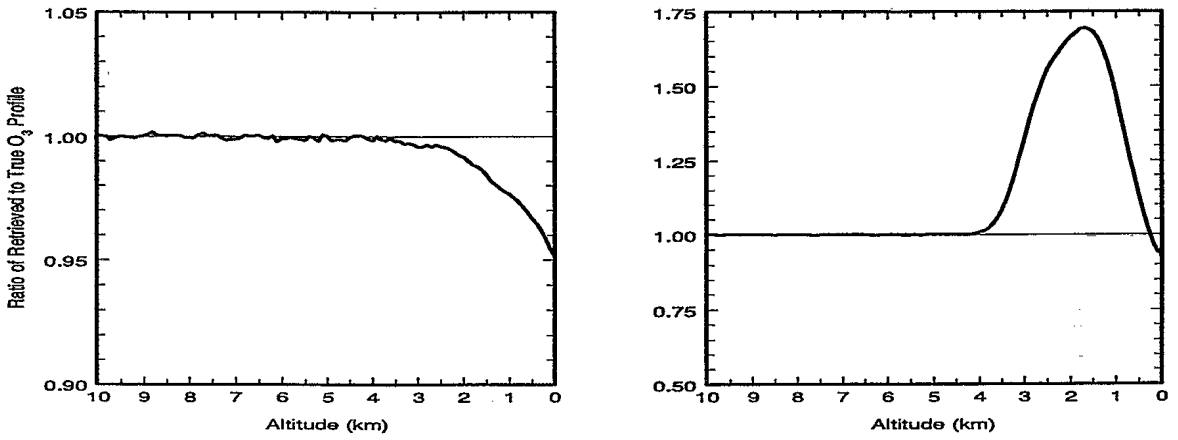


**Figure 3.** Ratio of retrieved to true ozone profile in the case of multiply scattered returns. All three single scattering corrections terms $T_m$, $T_\beta$ and $T_a$ were subtracted. Left panel: 25-km ground layer visibility; right panel: 5-km visibility.

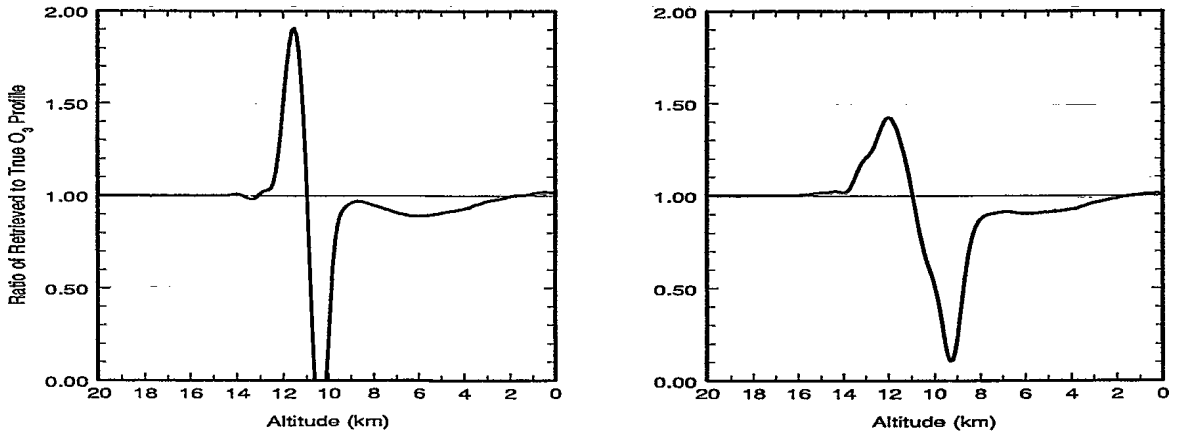


**Figure 4.** Ratio of retrieved to true ozone profile in the case of multiply scattered returns. All three single scattering corrections terms $T_m$, $T_\beta$ and $T_a$ were subtracted. Left panel: 2-km deep cold cirrus; right panel: 4-km deep cold cirrus. In both cases the cirrus optical depth is 1 and the ground visibility is 25 km.

in the form of cirrus clouds or low visibility ground haze layers, there is a need to correct for aerosol effects. In the case of single scattering, we have the explicit correction terms given by Eqs. 5-7 but, for multiple scattering, we depend on numerical methods as used here. In both instances, however, corrections would require simultaneous ozone and aerosol scattering measurements. It is noteworthy that the DIAL errors do not propagate beyond the regions of sufficiently dense aerosols. Hence, it appears that uncorrected $N_{O_3}$ profiles would still have acceptable precision outside of these regions. Finally, the simulations of this study were carried out for a space geometry. In ground-based measurements, the multiple scattering influence would definitely be less for the same system parameters.

## 3. BENEFIT

It has been recognized for quite some time[15–17] that retrievable information is contained in the multiple scattering contributions to lidar returns. In recent years, we have been developing at our laboratory measurement and inversion techniques[18–21] to take advantage of this, in particular to derive particle size data from lidar returns.

Our multiple scattering approach consists in measuring the lidar returns at multiple fields of view (MFOV). The signals at fields of view greater than the beam divergence are made up essentially of multiply scattered radiation. We have tried various measurement techniques that can be divided into two main categories: simultaneous and sequential recordings. Simultaneous recordings are best suited for fast changing conditions and are probably essential where scanning is required. However, the sequential approach is the cheapest and most adaptable, hence very convenient for research needs where some level of failure rate is acceptable.

Our general inversion method for exploiting multiple scattering is outlined in Ref. 20. It is applicable to scattering particles greater than the lidar wavelength, which at 1.06 $\mu$m is valid for fog, clouds and precipitation droplets. Under this condition, half of the particulate scattering is due to diffraction and is concentrated in a narrow peak centered on the laser axis. It follows that the multiply scattered radiation collected at small fields of view by a lidar receiver in a co-axial configuration has, for the most part, undergone a single backscattering at an angle close to 180° preceded and followed by near forward scatterings.[22] Hence, the field-of-view dependence of the lidar returns is strongly related to the profile of the scattering diffraction peak. Diffraction theory tells us that the angular width of the peak is inversely proportional to the average diameter of the droplets. As a result, the MFOV measurements contain retrievable information on the droplet size. Reference 20 describes the method used here to extract at each range of the MFOV returns the effective droplet diameter $d$ defined as the ratio of the third to the second order moment of the size distribution density function.

The solution for the extinction coefficient begins at the range $R_{ms}$ where multiple scattering becomes measurable. We use a second order scattering model to calculate at that point the optical depth $\tau(R_{ms}) = \int_0^{R_{ms}} \alpha(r)\mathrm{d}r$, where $\alpha$ is the extinction coefficient, in terms of the relative strength of the MFOV returns and the value $d(R_{ms})$ obtained as explained in the preceding paragraph. This constitutes sufficient information to solve the single scattering lidar equation for the extinction coefficient $\alpha(R)$ at all ranges $R \leq R_{ms}$. In addition, from the value of $d(R_{ms})$ and the assumption of a general form for the particles size density distribution, for example a modified gamma function in the cases of fog and cloud droplets, we calculate the backscatter-to-extinction coefficient $\beta/\alpha$ at $R_{ms}$ and thus determine $\alpha(R_{ms})$ and $\beta(R_{ms})$. Substituting in Eq. 1 for $P$, $\beta$ and $\alpha$, respectively, the measured return at the smallest field of view and the solutions just obtained for $\beta(R_{ms})$ and $\alpha(R \leq R_{ms})$, we then calibrate the complete lidar return, i.e. determine the instrument constant $KP_0$. With $KP_0$ known and the value of $d(R)$ computed by the method of the preceding paragraph, we finally solve for the extinction coefficient $\alpha(R > R_{ms})$ by substitution of the measured MFOV returns in the multiple scattering lidar equation derived in Ref. 11. The solutions for $d$ and $\alpha$ are nonlinearly coupled. In our algorithm, they are uncoupled by performing an iteration at each range step. Convergence is generally achieved in 2-4 cycles.

The overall inversion results are the range-resolved solutions for the effective particle diameter $d(R)$ and the extinction coefficient $\alpha(R)$ at the lidar wavelength. The solution for $d$ begins at the onset of multiple scattering where a clear field-of-view dependence becomes measurable. However, the solution for the extinction coefficient is calculated back to the origin by solving the single scattering lidar equation valid in that region.

An example of measurements and corresponding solutions is given in Fig. 5. On the left panel are plotted the raw returns for a small and a large field of view, and on the right panel the solutions for the extinction coefficient and droplet diameter. The lidar was pointed in a near vertical direction and the meteorological conditions were for a light rain under a 100% cloud cover. The large separation between the raw signals at altitudes below 120-140 m is caused

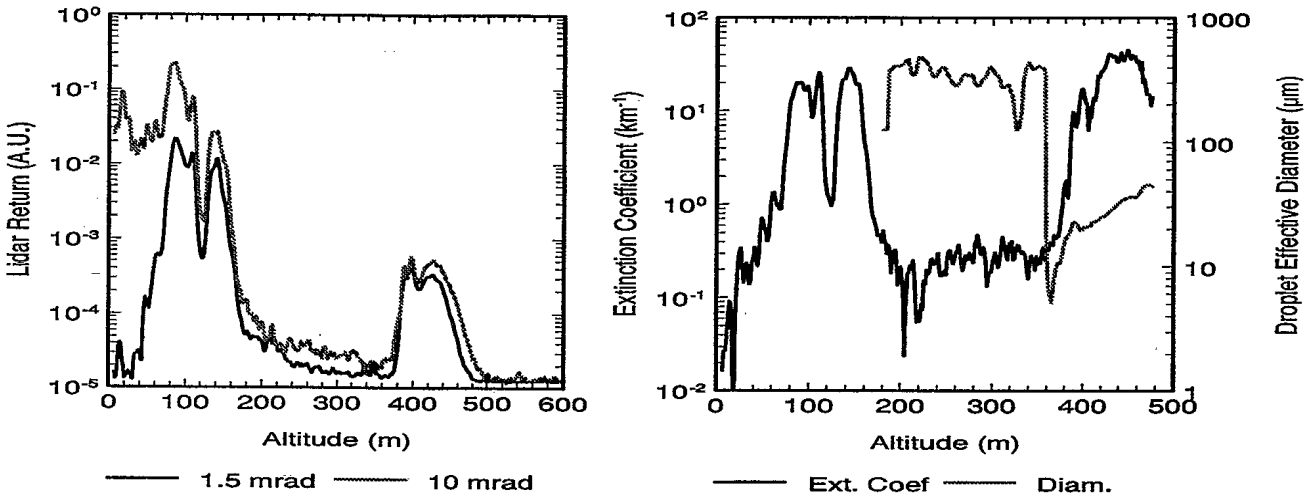


**Figure 5.** MFOV lidar signals (left panel) and derived solutions for extinction coefficient and effective droplet diameter (right panel); 12 February 1998, 09:40

by out-of-focus effects since the receiver telescope was set for the main cloud layer at 400 m. The out-of-focus effects are important at the narrow field of view but less so at the wide field of view since the latter collects the majority of the photons irrespective of whether they form a clear image or not. Although the solutions at low altitudes were calculated with the widest field-of-view return, they are neverthelesse suspicious below 40-50 m because the out-of-focus effects become very large. On the high altitude end, the solutions are terminated at 480 m where the narrowest field-of-view return reaches the noise level.

The extinction solutions show two distinct cloud layers, one at an altitude less than 100 m and the other at 400 m. The layer at 100 m was rather intermittent. In the five minutes preceding this measurement, it appeared and disappeared twice and, beginning with Fig. 5, it was continuously detected for a period of at least twenty minutes but with considerable fluctuations in height, density and thickness, and with much vertical structure as illustrated by the narrow double peaks of Fig. 5.

The cloud extinction in the two layers ranges from 20 to 50 $km^{-1}$, values that are consistent with general descriptions of stratus clouds. The solution below and between the cloud layers gives a more or less uniform rain extinction of 0.3 $km^{-1}$ in good agreement with ground observations. The effective droplet diameter is 300-400 $\mu$m for rain. In the main cloud layer, following a rapid transition undershoot that is probably an artefact of the calculation algorithm, it increases with height from about 20 to near 40 $\mu$m. These values are quite reasonable. The size solution is not calculated below 200 m because of uncertainties in the relative signal strength between the fields of view owing to the out-of-focus effects.

The main advantage of the proposed inversion method is that it provides simultaneous solutions for the extinction coefficient and the effective particle diameter without the need for additional independent inputs on a backscatter-to-extinction ratio and a boundary value. This is not only valuable intrinsic information but it gives us the means of estimating aerosol or cloud properties inaccessible from conventional lidar measurements, for example the extinction coefficients at other wavelengths, the particle density, the cloud liquid water content, etc. These are important outputs for various applications. Illustrative results giving the visible, mid and far infrared band transmittances, and the liquid water content calculated from the solutions of Fig. 5 are plotted in Fig. 6. It is shown that the visible and far infrared bands have transmittances similar as the lidar wavelength but that the mid infrared ends up being significantly more attenuated. The liquid water content values of 0.1 to 0.5 $g/m^3$ for the cloud layers are typical. In

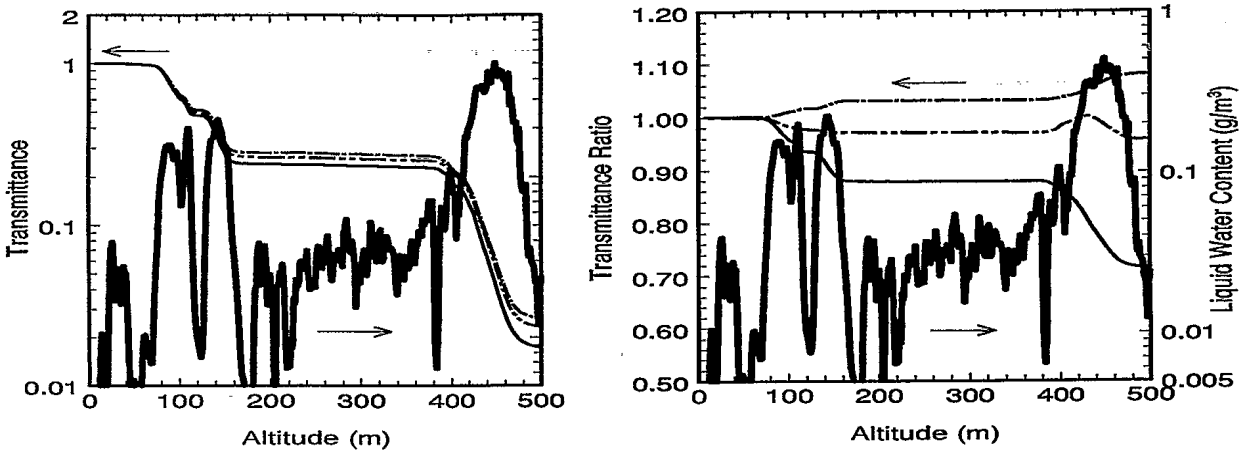


**Figure 6.** Liquid water content (both panels), band transmittances (left panel), and ratios of band-to-lidar transmittances (right panel) derived from the solutions of Fig. 5. Liquid water content (fat continuous curve) is read on the right vertical axes of both panels, all other quantities are read on the left vertical axes. Dot-dashed curves: visible band transmittance in left panel and ratio to lidar transmittance in right panel; continuous curves: mid infrared band transmittance in left panel and ratio to lidar transmittance in right panel; and dot-dot-dashed curves: far infrared band transmittance in left panel and ratio to lidar transmittance in right panel.

rain, the value of $\sim 0.03$ g/m$^3$ together with an estimated fall velocity of 2-3 m/s for the 400 $\mu$m effective droplet diameter obtained from Fig. 5 gives a rain rate betwen 0.23 and 0.35 mm/h or, from the Marshall-Palmer rain model, a visible extinction coefficient of 0.15 to 0.2 km$^{-1}$ compared with the 0.3 km$^{-1}$ value of the solution of Fig. 5. Note that visible band and lidar extinctions are essentially equal in rain. In other words, the rain extinction and liquid water content values of Figs. 5 and 6, respectively, are consistent within a factor of 2 with the Marshall-Palmer rain model.

## 4. CONCLUSION

We have shown through simple examples how multiple scattering can hurt or benefit lidar remote sensing of atmospheric parameters. The point we have tried to make is that there is a need for the development of multiple scattering correction and exploitation methods. A great deal of modeling work has already been accomplished and is still being pursued both outside and within the MUSCLE cooperation group. Nevertheless, there is still room for additional focused efforts toward solving specific application problems.

The results of the first part of this paper are a reminder that many current lidar methods need to be looked at to determine whether and how their retrieval results are affected by multiple scattering. The modeling tools to do this already exist but further specialized developments will be required where corrective measurement and data analysis procedures become necessary to maintain the validity and the precision of the solutions.

The second part of the paper illustrates that useful exploitation can be made of multiple scattering. More precisely, we have been able to use multiple scattering contributions, where measurable, not only to solve for the extinction coefficient without the need for external data on a boundary value and a backscatter-to-extinction ratio but to derive a valid estimate of the average or effective particle size. The results are still preliminary. The solution method used here lacks a rigourous formulation and further analytic work is definitely needed. The perspective of

enhanced capabilities should be a driving force. In particular, the remote retrieval of particle size and concentration is an important step forward in the development of a practical means of characterizing more fully the temporal and spatial evolution of fog, clouds and precipitation for a better understanding of numerous atmospheric problems.

The field of multiple scattering lidars is opened to innovations and, considering the traditional vitality of lidar research, no doubt that they will be forthcoming.

## REFERENCES


1. L. Elterman, "The measurement of stratospheric density distribution with searchlight technique," *J. Geophys. Res.* **58**, pp. 509-520, 1951.
2. L. Elterman, "Aerosol measurements in the troposphere and stratosphere," *Appl. Opt.* **5**, pp. 1769-1776, 1966.
3. K. Liou and R.M. Schotland, "Multiple backscattering and depolarization from water clouds for a pulsed lidar system," *J. Atmos. Sci.* **28**, pp. 772-784, 1971.
4. C.M.R. Platt, "Lidar and radiometer observations of Cirrus clouds," *J. Atmos. Sci.* **30**, pp. 1191-1204, 1973.
5. S.R. Pal and A.I. Carswell, "Multiple scattering in atmospheric clouds: lidar observations," *Appl. Opt.* **15**, pp. 1990-1995, 1976.
6. *Applied Physics*, Volume B60, Number 4, April 1995.
7. L.R. Bissonnette, P. Bruscaglioni, A. Ismaelli, G. Zaccanti, A. Cohen, Y. Benayahu, M. Kleiman, S. Egert, C. Flesia, P. Schwendimann, A.V. Starkov, M. Noormohammadian, U.G. Oppel, D.M. Winker, E.P. Zege, I.L. Katsev, and I.N. Polonsky, "Lidar multiple scattering from clouds," *Appl. Phys.* **B60**, pp. 355-362, 1995.
8. S.T. Shipley, D.H. Tracy, E.W. Eloranta, J.T. Trauger, J.T. Stroga, F.L. Roesler, and J.A. Weinman, "High spectral resolution lidar to measure optical scattering properties of atmospheric aerosols. 1: theory and instrumentation," *Appl. Opt.* **22**, pp. 3716-3724, 1983.
9. A. Ansmann, U. Wandinger, M. Riebesell, C. Weitkamp, and W. Michaelis, "Independent measurements of extinction and backscatter profiles in cirrus clouds by using a combined Raman elastic-backscatter lidar," *Appl. Opt.* **31**, pp. 7113-7131, 1992.
10. S.R. Pal and L.R. Bissonnette, "Multiple scattering effect on ozone retrieval from space-based DIAL measurements," accepted for publication in *Applied Optics*, 1998.
11. L.R. Bissonnette, "Multiple-scattering lidar equation," *Appl. Opt.* **35**, pp. 6449-6465, 1996.
12. I.L. Katsev, E.P. Zege, A.S. Prikhach, and I.N. Polonsky, "Efficient technique to determine backscattered light power for various atmospheric and oceanic sounding and imaging systems," *J. Opt. Soc. Am.* **A14**, pp. 1338-1346, 1997.
13. W. Steinbrecht and A.I. Carswell, "Evaluation of the effects of Mount Pinatubo aerosol on differential absorption lidar measurements of stratospheric ozone," *J. Geophys. Res.* **100**, pp. 1215-1233, 1995.
14. U. Wandinger, "Raman lidar, HSRL, and DIAL techniques: principles and multiple scattering problems," proceedings of Eight Int'l Workshop on Multiple scattering Lidar Experiments, published by Defence Research establishment Valcartier, pp. 93-97, March 1996.
15. R.J. Allen and C.M.R. Platt, "Lidar for multiple backscattering and depolarization observations," *Appl. Opt.* **16**, pp. 3193-3199, 1977.
16. S.R. Pal and A.I. Carswell, "Polarization properties of lidar scattering from clouds at 347 nm and 694 nm," *Appl. Opt.* **17**, pp. 2321-2328, 1978.
17. K. Sassen and R.L. Petrilla, "Lidar depolarization from multiple scattering in marine stratus clouds," *Appl. Opt.* **25**, pp. 1450-1459, 1986.
18. L.R. Bissonnette and D.L. Hutt, "Multiple scattering lidar," *Appl. Opt.* **29**, pp. 5045-5046, 1990.
19. D.L. Hutt, L.R. Bissonnette, and L. Durand, "Multiple field of view lidar returns from atmospheric aerosols," *Appl. Opt.* **33**, pp. 2338-2348 , 1994.
20. L.R. Bissonnette and D.L. Hutt, "Multiply scattered aerosol lidar returns: inversion method and comparison with *in situ* measurements," *Appl. Opt.* **34**, pp. 6959-6975, 1995.
21. G. Roy, L.R. Bissonnette, C. Bastille, and G. Vallée, "Estimation of cloud droplet size density distribution from multiple-field-of-view lidar returns," *Opt. Eng.* **36**, pp. 3404-3415, 1997.
22. F. Nicolas, L.R. Bissonnette, and P.H. Flamant, "Lidar effective multiple-scattering coefficients in cirrus clouds," *Appl. Opt.* **36**, pp. 3458-3468, 1997.

#510080